UNIVERSIDADE DE SÃO PAULO

INSTITUTO DE FÍSICA
CAIXA POSTAL 20516
01498-970 SÃO PAULO - SP
BRASIL

PUBLICAÇÕES

IFUSP/P-1012

ELECTRON-ELECTRON BOUND STATES IN QED_3

H. O. Girotti, M. Gomes, J. L. deLyra, R. S. Mendes, J. R. S. Nascimento
Instituto de Física, Universidade de São Paulo

A. J. da Silva
Center for Theoretical Physics
Massachusetts Institute of Technology
Cambridge, MA 02139

Setembro/1992

Electron–Electron Bound States in QED$_3$*

H. O. Girotti†, M. Gomes, J. L. deLyra,
R. S. Mendes, J. R. S. Nascimento
Instituto de Física, Universidade de São Paulo
Caixa Postal 20516, 01498 - São Paulo, SP, Brazil.
and
A. J. da Silva‡
Center for Theoretical Physics,
Massachusetts Institute of Technology
Cambridge, MA 02139.

Abstract

This paper is dedicated to the study of the existence and the properties of electron-electron bound states in QED$_3$. A detailed analysis of the infrared structure of the perturbative series of the theory is presented. We start by analyzing the two-point Green's function, in the Bloch-Nordsieck approximation. The theory appears to be plagued by severe infrared divergencies, which nevertheless disappear when vacuum-polarization effects are non-perturbatively taken into account. The dynamical induction of a Chern-Simons term is at the root of this mechanism.

From the inspection of the electron-electron non-relativistic potential it then follows that equally charged fermions may either repel or attract and, moreover, that bound states do in fact exist in the theory. We calculate numerically the binding energies and average radius of the bound states. We find an accidental quasi-degeneracy of the ground state of the system, between the lowest-energy $l = -3$ and $l = -5$ states, which could be related to a radio-frequency resonance in high-T_c superconductors.

*Supported in part by Conselho Nacional de Desenvolvimento Científico e Tecnológico (CNPq) and by Fundação de Amparo à Pesquisa do Estado de São Paulo (FAPESP), Brazil.

†On leave of absence from Instituto de Física, Universidade Federal do Rio Grande do Sul, Caixa Postal 15051, 91500 - Porto Alegre, RS, Brazil.

‡On leave of absence from Instituto de Física, Universidade de São Paulo, Caixa Postal 20516, 01498 - São Paulo, SP, Brazil.

1 Introduction

As is well-known [1], the Maxwell-Chern-Simons (MCS) theory is a $(2+1)$-dimensional model describing the coupling of charged fermions $(\bar{\psi}, \psi)$ of mass m and electric charge e to the electromagnetic potential A_μ via the Lagrangian density

$$\begin{aligned}\mathcal{L} &= -\frac{1}{4}F_{\mu\nu}F^{\mu\nu} + \frac{\theta}{4}\epsilon^{\mu\nu\alpha}F_{\mu\nu}A_\alpha - \frac{1}{2\lambda}(\partial_\mu A^\mu)(\partial_\nu A^\nu) \\ &\quad + \frac{i}{2}\bar{\psi}\gamma^\mu\partial_\mu\psi - \frac{i}{2}(\partial_\mu\bar{\psi})\gamma^\mu\psi - m\bar{\psi}\psi + e\bar{\psi}\gamma^\mu A_\mu\psi, \qquad (1)\end{aligned}$$

where $F_{\mu\nu} \equiv \partial_\mu A_\nu - \partial_\nu A_\mu$, θ is a topological parameter with dimension of mass and λ is a gauge-fixing parameter. Neither parity nor time reversal are, separately, symmetries of the model[1]. The lowest order perturbative contribution to the effective fermion-fermion low-energy potential, arising from (1), was recently computed [2] and reads

$$V(\vec{r}) = \frac{e}{2\pi}\left(1 - \frac{\theta}{m}\right)K_0(|\theta|r) - \frac{e}{\pi\theta}\frac{1}{mr^2}\left[1 - |\theta|rK_1(|\theta|r)\right]L. \qquad (2)$$

Here, $\vec{r}$ is the relative distance between the electrons, $r = |\vec{r}|$, $L = r_1p_2 - r_2p_1$ is the orbital angular momentum, whose eigenvalues are denoted by l, $\vec{p}$ is the relative linear momentum of the electrons, and K_0 and K_1 designate the modified Bessel functions[2].

The linear dependence of V on L accounts for the breaking of parity and time reversal invariance in the non-relativistic approximation. The aim in Ref. [2] was to determine whether the potential (2) could bind a pair of identical fermions. For positive values of θ, a numerical solution of the Schrödinger equation confirmed the existence of a bound state for $e^2/(\pi\theta) = 500$, $m/\theta = 10^5$ and $l = 1$. Further numerical analysis indicated that all identical-fermion bound states are located in the region $e^2/(\pi\theta) > 1$.

Thus, we were naturally led to consider the limit $\theta \to 0$ where the MCS theory degenerates into QED$_3$, whose Lagrangian is

$$\mathcal{L} = -\frac{1}{4}F_{\mu\nu}F^{\mu\nu} - \frac{1}{2\lambda}(\partial_\mu A^\mu)(\partial_\nu A^\nu) + \frac{i}{2}\bar{\psi}\gamma^\mu\partial_\mu\psi - \frac{i}{2}(\partial_\mu\bar{\psi})\gamma^\mu\psi - m\bar{\psi}\psi + e\bar{\psi}\gamma^\mu A_\mu\psi. \qquad (3)$$

[1]Throughout this paper we use natural units ($c = \hbar = 1$). Our metric is $g_{00} = -g_{11} = -g_{22} = 1$, while for the γ-matrices we adopt the representation $\gamma^0 = \sigma_3, \gamma^1 = i\sigma^1, \gamma^2 = i\sigma^2$; $\sigma^i, i = 1, 2, 3$ are the Pauli spin matrices.

[2]The potential (2) looks similar to the one derived by Kogan [3] for the same problem. There are some important differences, however, that we would like to stress. The derivation in Ref. [2] is solely based on relativistic quantum field theory [4]. On the other hand, in Ref. [3] the corresponding potential is determined in two steps. First, the A_μ vector created by a point charge is computed. Then, the quantum mechanical Hamiltonian describing the low energy relative motion of the two electrons is assumed to be that of a charged particle in the presence of the external field A_μ. As a consequence, an extra term proportional to $[1 - |\theta|rK_1(|\theta|r)]^2$ arises in the formulation of Ref. [3].

Power counting indicates that the S-matrix elements of QED_3 are plagued with infrared singularities whose degree of divergence grows with the order of the perturbative expansion. The situation is, therefore, more severe than in QED_4 where all (on-shell) infrared divergences are logarithmic. Hence, the usual mechanism (soft bremsstrahlung) for cancelling infrared divergences at the level of the cross section fails, since it would only be operative for the leading divergence. Furthermore, a non-perturbative analysis of the two-point fermion Green function $G(p)$, carried out within the Bloch-Nordsieck (BN) [5–8] approximation, shows that G is well defined for generic values of the momentum p but develops an essential on-shell singularity. Through a multiplicative renormalization, $G \to G_R = Z^{-1}G$, one may define a new Green function behaving on shell as a simple pole. However, G_R is found to exhibit an essential off-shell singularity which reintroduces the difficulty for the scattering amplitudes. All these developments are presented in Sec. 2.

We recall next that the BN approximation does not take into account vacuum polarization effects. This does not constitute a serious limitation for QED_4, as far as the infrared structure of the theory is concerned. In fact, for QED_4 these diagrams are, on the one hand, free from infrared singularities while, on the other hand, they do not give rise to a mechanism for dynamical mass generation. In contrast to this, when vacuum polarization effects are non-perturbatively incorporated into the photon propagator, the infrared behavior of QED_3 changes drastically, as is demonstrated in Sec. 3. Essentially, the theory is reformulated in terms of a massive vector boson whose mass is $|\theta| = e^2/(8\pi)$, the dynamically induced Chern-Simons term [1,9] being at the root of this mechanism. Thus, the infrared disease afflicting perturbative QED_3 is cured and one is allowed to read off the corresponding effective electron-electron low-energy potential directly from Eq. (2), after replacing $\theta \to -e^2/(8\pi)$. Hence,

$$eV^{\mathrm{QED}_3}(\vec{r}) = \frac{e^2}{2\pi}\left(1+\frac{e^2}{8\pi m}\right)K_0\left(\frac{e^2}{8\pi}r\right)+\frac{8}{mr^2}\left[1-\frac{e^2}{8\pi}rK_1\left(\frac{e^2}{8\pi}r\right)\right]L. \qquad (4)$$

The terms proportional to K_0 in Eq. (4) are both repulsive. The term $8L/(mr^2)$ becomes attractive (repulsive) for negative (positive) eigenvalues of L, while the term proportional to K_1 acts in the opposite way. Hence, unlike the case of QED_4, electrons may repel or attract in QED_3, the infrared structure of the theory being responsible for this unusual behavior of the interaction between equally charged particles. A numerical investigation on whether the potential (4) can sustain electron-electron bound states is presented in Sec. 4. There we show that such bound states do in fact exist. For some of them the corresponding dissociation temperature will be seen to be in qualitative agreement with the values encountered for the critical temperature of high-T_c superconductors.

Our conclusions are contained in Sec. 5. A preliminary version of some of the results presented in this paper is contained in Ref. [10].

We remind the reader that the signs of the electron's spin and of the induced topological mass are both equal to the sign of the fermionic mass term in the Lagrangian (3) [1]. Thus, in a theory involving both spin-up and spin-down fermions there will be no induced Chern-

Simons term and, for the specific case of electrodynamics, there will be no cure for the infrared problem. This explains why it is essential that we restrict ourselves, in this paper, to the case of a single two-component fermion field. The generalization to the case of several flavors is straightforward and will be mentioned along the way.

2 Infrared Structure

As we already mentioned in the Introduction, power counting alone reveals that perturbative QED_3 is afflicted by severe on-shell infrared singularities. To gain some insight into the infrared structure of this theory, we shall start by computing the two-point fermionic Green function in the BN approximation. To keep the singularities under control, we approach QED_3 as the $\theta \to 0$ limit of the MCS theory (1). Clearly, both theories exist off shell and MCS goes into QED_3 as $\theta \to 0$.

The BN approximation consists of the replacement of the γ^μ-matrices in Eq. (1) by a vector u^μ, with $u^2 = 1$. As a consequence, the usual free fermion propagator is replaced by the retarded function

$$\begin{aligned} G_F(x-y) &\equiv \frac{1}{(2\pi)^3}\int d^3p\,\frac{e^{-ip\cdot(x-y)}}{u\cdot p - m + i\epsilon} \\ &= -iu^0 H(x^0-y^0)e^{-i\frac{m}{u^0}(x^0-y^0)}\delta^{(2)}\left[\vec{u}(x^0-y^0)-u^0(\vec{x}-\vec{y})\right], \end{aligned} \qquad (5)$$

where $H(x^0)$ is the Heaviside step function. Then, the interaction does not imply any corrections to the vector meson propagator. For our present purposes this does not represent a serious drawback since vacuum polarization insertions do not alter the leading infrared behavior of a graph.

The Green functions of the theory will be computed by functionally differentiating the generating functional $U_0[J_\mu, \eta, \bar{\eta}]$ with respect to the external sources. In this paper, J_μ and η, $\bar{\eta}$ denote the vector meson and fermion external sources, respectively. After integration on the fermionic degrees of freedom one finds

$$\begin{aligned} U_0[J_\mu,\eta,\bar{\eta}] &= \mathcal{N}\int[\mathcal{D}A_\mu]e^{\mathcal{D}}\exp\left\{iS[A]-\frac{i}{2\lambda}\int d^3x(\partial_\mu A^\mu)^2\right. \\ &\left. + i\int d^3x\,J_\mu(x)A^\mu(x) - i\int d^3x\int d^3y\,\bar{\eta}(x)G[A|x,y]\eta(y)\right\}, \end{aligned} \qquad (6)$$

where $e^{\mathcal{D}}$ is the fermionic determinant, $S[A] = -F_{\mu\nu}F^{\mu\nu}/4$ and $G[A|x,y]$ is the fermionic two-point Green function in the presence of an external field A_μ.

The solubility of the model in the BN approximation is partly due to the fact that the A_μ propagator is not corrected by the interaction, and partly due to the factorization property of $G[A|x,y]$. In fact, one can convince oneself that the differential equation

$$\left\{iu^\mu\left[\partial_{x_\mu} - ieA_\mu(x)\right] - m\right\} G[A|x,\, y] = \delta^{(3)}(x-y)$$

is solved by

$$G[A|x,\, y] = h[A|x] G_F(x-y) h^{-1}[A|y], \tag{7}$$

where

$$h[A|x] = \exp\left[ie\int d^3z\, \xi^\mu(x-z) A_\mu(z)\right],$$

and

$$\xi^\mu(x) = \frac{i}{(2\pi)^3}\int d^3k \frac{u^\mu}{(u\cdot k)} \mathrm{e}^{-ik\cdot x}.$$

One can check that expression (7) can be cast in a form analogous to that quoted in Ref. [6] for the case of QED_4.

Formally, the computation of D yields $D = \int_0^e de' \int d^3x G[A|x,x] u^\mu A_\mu(x)$, which in view of (7) reduces to

$$D = e\int d^3x\, G_F(x,x) u^\mu A_\mu(x),$$

showing that D can, at most, depend linearly on A_μ. However, as seen from (5), $G_F(x,x)$ is ambiguous. In the original model, with γ^μ instead of u^μ, Lorentz invariance demands the vanishing of the tadpole contribution to the fermionic determinant. Based on this fact we shall therefore take, from now on, $D = 0$.

The complete two-point fermion Green function can now be readily found,

$$\begin{aligned} G(x,y;m,\theta) &\equiv \frac{1}{U_0[0]}\frac{1}{i^2}\frac{\delta^2 U_0[J_\mu = 0,\eta,\bar\eta]}{\delta\bar\eta(x)\,\delta\eta(y)}\bigg|_{\eta=\bar\eta=0} \\ &= iG_F(x-y)\exp\left[-\frac{i}{2}e^2\int d^3z\int d^3z' S_\mu(x,y;z)\Delta^{\mu\nu}(z,z') S_\nu(x,y;z')\right], \end{aligned}$$

where

$$S^\mu(x,y;z) \equiv \xi^\mu(x-z) - \xi^\mu(y-z),$$

and $i\Delta^{\mu\nu}$ is the photon propagator. From (6) it follows that, in momentum space,

$$i\tilde\Delta^{\mu\nu}(k,\theta) = -\frac{i}{k^2-\theta^2}\left(g^{\mu\nu} - \frac{k^\mu k^\nu}{k^2}\right) - \frac{\theta}{k^2-\theta^2}\frac{\epsilon^{\mu\nu\rho}k_\rho}{k^2} - i\lambda\frac{k^\mu k^\nu}{(k^2)^2}. \tag{8}$$

Hence, for the Fourier transform $G(p;m,\theta) \equiv \int d^3x \exp(ipx) G(x;m,\theta)$ one gets, after some algebra,

$$G(p;m,\theta) = \int_0^\infty d\nu \exp\left[i\nu(u\cdot p - m + i\epsilon) + f(\nu,\theta)\right],$$

where

$$f(\nu,\theta) = -\frac{ie^2}{(2\pi)^3}\int d^3k\{1-\cos[\nu(u\cdot k)]\} U(k,\theta), \tag{9}$$

and

$$U(k,\theta) \equiv \frac{u^\mu \tilde\Delta_{\mu\nu}(k,\theta) u^\nu}{(u\cdot k)^2}.$$

Since $u^\mu \epsilon_{\mu\nu\rho} u^\nu = 0$, the second term in (8) does not contribute to $U(k,\theta)$. Thus, the $\theta \to 0$ limit of G in the MCS theory is the same as that of the corresponding function in massive QED_3.

The behavior of the integrand in Eq. (9) in the limit $k \to \infty$, with $u\cdot k$ kept constant, tells us that $f(\nu,\theta)$ develops a logarithmic ultraviolet divergence. This divergence, which can be absorbed into a mass renormalization, is entirely due to the approximation being used (u^μ instead of γ^μ)[3]. The two-point Green function G in terms of the renormalized mass m_R turns out, then, to be given by

$$\begin{aligned} G(p;m_R,\theta) &= \frac{1}{\theta}\int_0^\infty dv \\ &\exp\left\{iv\left[i\epsilon + \frac{Q}{\theta} - \frac{e^2}{4\pi\theta}\left(\ln\frac{M}{\theta} + \frac{\mathrm{e}^{-iv}-1}{iv} + 2\frac{\mathrm{e}^{-iv}-1+iv}{(iv)^2} + Ei(-iv) - \lambda\right)\right]\right\}, \end{aligned} \tag{10}$$

where $Q \equiv u\cdot p - m_R$, $Ei(z)$ is the exponential-integral function,

$$m_R = m + \frac{e^2}{4\pi}\ln\left(\frac{\Lambda}{M}\right), \tag{11}$$

Λ is an ultraviolet cutoff, and M plays the role of a subtraction point[4]. For $\theta \neq 0$, the singularity structure of $G(p;m_R,\theta)$ can be seen to consist of a pole at

$$u\cdot p = m_R + \frac{e^2}{4\pi a^2}\left(\ln\frac{M}{\theta} - \lambda a^2\right),$$

[3] A similar situation arises in QED_4 where the corresponding function $f(\nu)$ presents linear and logarithmic ultraviolet divergences, the linear divergence being induced by the replacement $\gamma^\mu \to u^\mu$ [6].

[4] An analogous situation arises in the one-loop calculation of Ref. [1], where a gauge-dependent contribution to the electron mass is found.

plus branch cuts. If one insists in keeping the pole of G at the renormalized mass defined in Eq. (11), one must choose $M = \theta \exp(\lambda)$, thus lumping all the gauge dependence of G into the subtraction point. Moreover, the Green function G can be renormalized,

$$G(p; m_R, \theta) \to G_R(p; m_R, \theta) \equiv Z^{-1} G(p; m_R, \theta),$$

such that

$$\lim_{u\cdot p \to m_R} (u \cdot p - m_R) G_R(p; m_R, \theta) = i.$$

It may be checked that the ultraviolet-finite renormalization constant

$$Z = \exp\left(-\frac{e^2}{4\pi a^2 \theta}\right)$$

does the job. Everything runs smoothly for $\theta \neq 0$.

However, the above scheme does not survive the limit $\theta \to 0$. While the pole of G_R can be kept at the value of the renormalized mass, the constant Z presents an essential singularity which in turn is transferred to G_R and shows up for all off-shell values ($u \cdot p \neq m_R$) of the momentum. One may try to circumvent this difficulty by defining the two-point fermion Green function of QED$_3$ as the $\theta \to 0$ limit of (10), keeping M arbitrary. For $Q < 0$ and after a Wick-like rotation one arrives at

$$G(p; m_R, \theta = 0) = \frac{i}{Q} \int_0^\infty dv \exp\left\{-v + \frac{e^2}{4\pi Q} v \left[C + \ln\left(-\frac{M}{Q} v\right) - \lambda\right]\right\}, \qquad (12)$$

where C is the Euler constant. On the other hand, if $Q > 0$ one obtains

$$G(p; m_R, \theta = 0) = -\frac{i}{Q} \int_0^\infty dv \exp\left\{v - \frac{e^2}{4\pi Q} v \left[C + \ln\left(\frac{M}{Q} v\right) - \lambda\right]\right\}, \qquad (13)$$

although in this last case the Wick-like rotation is only allowed if $e^2 \neq 0$. Expressions (12) and (13) are well defined for generic values of Q but contain an essential singularity at $Q = 0$[5].

In both cases above, the BN approximation fails to provide an acceptable functional form for the two-point fermion Green function of QED$_3$. This is an indication that the infrared singularities occurring in each order of perturbation theory do not add up to a finite limit. Moreover, the inclusion of soft bremsstrahlung emission, which in QED$_4$ removes the infrared problem from the cross sections, is of no help in the present case since it would only act on the leading divergences. Nothing changes, qualitatively, if vacuum polarization insertions are added order by order in perturbation theory. Nevertheless, when vacuum polarization effects are non-perturbatively incorporated into the photon propagator, a photon mass is dynamically generated and as a consequence the infrared disease is cured. To show how this comes about is the purpose of the next section.

[5]It is instructive to compare this result with the corresponding one in QED$_4$, where the two-point fermion Green function exhibits a power law behavior in the variable Q [6].

3 Vacuum Polarization Effects

The lowest-order graph contributing to the vacuum polarization tensor $\Pi^{\rho\sigma}$ yields

$$\Pi^{\rho\sigma}(q) = ie^2 \int \frac{d^3k}{(2\pi)^3} \frac{\mathrm{Tr}[\gamma^\rho(\not{k} + \not{q} + m)\gamma^\sigma(\not{k} + m)]}{[(q+k)^2 - m^2](k^2 - m^2)}.$$

Since we are interested in the quantum corrections to a non-relativistic potential, we shall retain only those terms which are zero and first order in q. Gauge invariance alone ensures that $\Pi^{\rho\sigma}(0) = 0$. For the first-order contribution, which gives origin to the induced Chern-Simons term [1,9], one finds

$$\Pi^{(1)}_{\rho\sigma}(q) = -i\frac{e^2}{8\pi} \epsilon_{\rho\sigma\mu} q^\mu.$$

We emphasize that $\Pi^{(1)}_{\rho\sigma}(q)$ is ultraviolet-finite and that, therefore, no regularization is needed for its computation. Alternatively, if one adopts the point of view that ultraviolet divergences should be kept under control by the regularization of the entire theory, the result quoted in this last equation is true only if a parity-time reversal invariant regularization is used.

We now modify the photon propagator by resumming the geometric series resulting from the iteration of $\Pi^{(1)}_{\rho\sigma}$ (see Fig. 1). This is formally equivalent to adding to the Lagrangian (3) the term

$$\mathcal{L}_{CS} = -\frac{e^2}{32\pi} \epsilon^{\mu\nu\rho} F_{\mu\nu} A_\rho,$$

which is nothing but a Chern-Simons term with and induced topological mass

$$\theta_{in} = -\frac{e^2}{8\pi}. \qquad (14)$$

Hence, in the low-energy regime, the theory effectively describes the interaction of fermions with massive vector particles of mass $|\theta_{in}|$ and is, therefore, free from infrared problems. Moreover, from Eqs. (2) and (14) it follows that the QED$_3$ effective electron-electron low-energy potential is, in fact, the one given in Eq. (4).

We verify the consistency of the present formulation of QED$_3$ by showing that all remaining contributions to V^{QED_3} are, up to some power of $\ln(e^2/m)$, of order e^2/m or higher with respect to (4), and vanish as $e^2/m \to 0$. To see how this comes about, we compute the vertex correction Λ^μ to V^{QED_3} arising from the diagram in which only one massive vector particle is exchanged[6] (see Fig. 2). After the replacement $\theta \to \theta_{in}$, the massive vector field propagator can be read off directly from Eq. (4) of Ref. [2],

[6]For the vertex corrections in MCS theory see Ref. [11]. We would like to point out, however, that the limit $\theta \to 0$ in the MCS theory differs radically from the limit $\theta_{in} = -e^2/(8\pi) \to 0$ in QED$_3$, since in the latter case the vanishing of the topological mass also implies the vanishing of the coupling constant.

$$D_{\mu\nu}(k) = \frac{-i}{k^2 - \theta_{in}^2}\left(P_{\mu\nu} \; - \; i\theta_{in}\epsilon_{\mu\nu\rho}\frac{k^\rho}{k^2}\right) - i\lambda\frac{k_\mu k_\nu}{k^4}f(k^2),$$

where $P_{\mu\nu} \equiv g_{\mu\nu} - k_\mu k_\nu/k^2$, and an arbitrary function $f(k^2)$ has been incorporated into the longitudinal part. Accordingly, Λ^μ can be split as follows

$$\Lambda^\mu = \Lambda^\mu_g + \Lambda^\mu_\epsilon + \Lambda^\mu_L,$$

where the subscripts g, ϵ, and L make reference to those pieces of $D_{\mu\nu}$ proportional to $g_{\mu\nu}$, $\epsilon_{\mu\nu\rho}k^\rho$ and $k_\mu k_\nu$, respectively. The computation of Λ^μ_L is straightforward and yields

$$\Lambda^\mu_L = i\lambda\bar{v}^{(+)}(\mathbf{p}_1')\gamma^\mu v^{(-)}(\mathbf{p}_1)\int\frac{d^3k}{(2\pi^3)}\frac{f(k^2)}{k^2},$$

where, as in Ref. [2], $v^{(-)}(\mathbf{p}_1)$ ($\bar{v}^{(+)}(\mathbf{p}_1')$) is a two-component spinor describing a free electron of two-momentum $\mathbf{p}_1$ ($\mathbf{p}_1'$) in the initial (final) state. Since Λ^μ_L does not depend on the momentum transfer $q \equiv p_1' - p_1$, it can be absorbed into the wave-function renormalization constant. When computing Λ^μ_g and Λ^μ_ϵ only zero- and first-order terms in q/m will be retained, since our interest here is restricted to the non-relativistic regime. Furthermore, all the momentum integrals over loops are ultraviolet-finite and there is no need for regularization. After absorbing the zero-order terms into the wave-function renormalization constant, one arrives at

$$\Lambda^{\mu(1)}_g(q) = \frac{N_g}{16\pi}\frac{e^2}{m}\epsilon^{\mu\nu\rho}\frac{q_\nu}{m}\,\bar{v}^{(+)}(\mathbf{p}_1')\gamma_\rho v^{(-)}(\mathbf{p}_1), \tag{15}$$

and

$$\Lambda^{\mu(1)}_\epsilon(q) = -\frac{N_\epsilon}{16\pi}\frac{e^2}{m}\epsilon^{\mu\nu\rho}\frac{q_\nu}{m}\,\bar{v}^{(+)}(\mathbf{p}_1')\gamma_\rho v^{(-)}(\mathbf{p}_1), \tag{16}$$

where

$$N_g = -3 + 3\frac{e^2}{8\pi m} + 2\left[1 - \frac{3e^4}{(16\pi m)^2}\right]\ln\left(1 + \frac{16\pi m}{e^2}\right), \tag{17}$$

and

$$N_\epsilon = -\frac{e^2}{\pi m}\ln\left(1 + \frac{16\pi m}{e^2}\right). \tag{18}$$

From Eqs. (15–18) it follows that $\Lambda^{\mu(1)}(q)$ behaves as $(e^2/m)\ln(e^2/m)$ when $e^2/m \to 0$ ($\theta_{in}/m \to 0$), while power-counting indicates that the full vertex insertion $\Lambda^\mu(q)$ (Fig. 2) may diverge logarithmically at the just mentioned infrared limit. The fact that $\Lambda^{\mu(1)}(q)$ exhibits an improved infrared behavior is not a peculiarity of the particular insertion under

analysis but applies to any vertex part involving an arbitrary number of exchanged massive vector particles. Indeed, the leading infrared divergence of any of these parts only shows up in those terms containing even powers of the momentum transfer q, as can be seen by setting to zero the loop momenta in the numerators of the corresponding Feynman integrals. Thus, the terms linear in q exhibit a milder infrared behavior.

By using the technique described in Ref. [2] one finds the correction $\Delta V^{\mathrm{QED_3}}$ arising from the diagrams in Fig. 3,

$$\begin{aligned} e\Delta V^{\mathrm{QED_3}} &= \frac{e^2}{8\pi}\frac{e^2}{m}(N_g - N_\epsilon) \\ &\times \left[\frac{e^2}{16\pi^2 m}\left(1 + \frac{e^2}{8\pi m}\right)K_0\left(\frac{e^2}{8\pi}r\right) - \frac{\delta^2(\mathbf{r})}{m^2} + \frac{e^2}{8\pi^2 m^2}K_1\left(\frac{e^2}{8\pi}r\right)\frac{L}{r}\right]. \end{aligned} \tag{19}$$

From Eqs. (17–19) it follows that $e\Delta V^{\mathrm{QED_3}}$ also behaves as $(e^2/m)\ln(e^2/m)$ when $e^2/m \to 0$, and turns out to be negligible if $e^2/m \ll 1$. This establishes the region of validity of our approximations.

4 Electron-Electron Bound States

We turn next to the investigation of the existence and properties of bound states of two identical fermions of mass m and charge e interacting through the non-relativistic potential $V^{\mathrm{QED_3}}$ given in (4). The corresponding radial Schrödinger equation is found to read

$$\mathcal{H}_l R_{nl}(y) = \epsilon_{nl}R_{nl}(y),$$

where R_{nl} is the radial part of the wave function, l is, as defined before, the angular momentum eigenvalue, n is the principal quantum number, and $\mathcal{H}_l$ is the effective radial Hamiltonian, namely,

$$\mathcal{H}_l R_{nl}(y) = -\left[\frac{\partial^2 R_{nl}(y)}{\partial y^2} + \frac{1}{y}\frac{\partial R_{nl}(y)}{\partial y}\right] + U_l^{eff}(y)R_{nl}(y).$$

Here U_l^{eff} denotes the effective radial potential arising from (4),

$$U_l^{eff}(y) = \frac{l^2}{y^2} + \frac{\alpha_{in}}{2}\left(1 + \beta_{in}\right)K_0(y) + \frac{\alpha_{in}l}{y^2}\left[1 - yK_1(y)\right], \tag{20}$$

where we introduced the dimensionless parameters $y = e^2 r/(8\pi)$, $\alpha_{in} = e^2/(\pi|\theta_{in}|) = 8$, $\beta_{in} = m/|\theta_{in}| = 8\pi m/e^2$, and $\epsilon_{nl} = 64\pi^2 m E_{nl}/e^4$, E_{nl} being the energy eigenvalue.

A straightforward analysis of (20) reveals that electron-electron bound states are possible only for $l = -1$, -3, -5 and -7. In order to see this, we consider the derivative

$$\frac{\partial U_l^{eff}(y)}{\partial y} = -\frac{2l(l+\alpha_{in})}{y^3} + \frac{\alpha_{in} l}{y} K_0(y) - \left[\frac{\alpha_{in}}{2}(1+\beta_{in}) - \frac{2\alpha_{in} l}{y^2}\right] K_1(y).$$

For l negative and outside the interval $[-7,-1]$, this derivative is negative definite and, therefore, U_l^{eff} has no local minima. Inside this interval, on the other hand, an examination of the behavior of U_l^{eff} reveals that for small y it diverges to $+\infty$, while for large y it approaches zero from negative values. It then follows that U_l^{eff} has an absolute minimum, thus opening up the possibility for bound states. The fact that Fermi statistics requires that l be odd reduces the possibilities to the values mentioned above. Had we chosen the negative sign for m we would have obtained $\theta_{in} = +e^2/(8\pi)$ and bound states, with identical energy eigenvalues, would be possible for $l = +1, +3, +5$ and $+7$. This analysis can be easily extended to the case of two different flavors. If the electrons are in an antisymmetric flavor state, bound states may emerge for $l = -2, -4$ and -6.

The straight numerical resolution of the Schrödinger equation is useful for determining quickly whether bound states exist or not, but it is not so useful for the determination of the binding energies of such bound states. The reason is that in order to solve the equation one needs, beforehand, a definite value for the energy parameter. Since the energy eigenvalue is not known a priori, one must search for it, solving the equation repeatedly by starting with the boundary condition for R_{nl} at $y = 0$, and propagating the wave function forward until one realizes the boundary condition for large y. Besides being a difficult process in itself, due to the very sensitive dependence of the asymptotic behavior of the wave function on the value of the energy parameter, it interacts in a complex way with the finiteness of the integration interval and of the integration range.

The existence of bound states for the potential given in (20) was examined numerically by means of a stochastic variational algorithm. We found this method much more convenient than the resolution of the complete eigenvalue problem, which is large and hard. The variational algorithm consists of a direct search for the lowest eigenvalues only, and is therefore more appropriate for our purposes. In all cases which were examined with both this procedure and the Schrödinger equation, the results were the same, within the numerical limitations of each method. With the variational algorithm we were able to quickly identify, for a given l, the state of minimum energy ($n = 0$), for a variety of values of β_{in}, and to estimate roughly the binding energies. However, for a precise determination of the binding energies, long double-precision runs were necessary. We also measured the expectation value $(\bar{r}_{nl})$ of the radius in the state thus obtained. A typical configuration of R_{0l}, and the corresponding potential, are displayed in Fig. 4.

In the variational algorithm we varied the wave function R_{0l}, subject to the boundary condition $R_{0l}(0) = 0$, while trying to decrease the energy of the state, which is given by

$$\epsilon_{0l} = \frac{\int_0^\infty dy\, y \left\{\left[\frac{\partial R_{0l}(y)}{\partial y}\right]^2 + U_l^{eff}(y) R_{0l}(y)^2\right\}}{\int_0^\infty dy\, y\, R_{0l}(y)^2}.$$

During the variation of the wave function, besides implementing the boundary condition at the origin, we kept constant its maximum value. This implies that the normalization of the wave function relaxes to some arbitrary value. The requirement that the wave function should decrease exponentially for large values of y was realized automatically by the algorithm.

In order to be able to represent the wave function R_{0l} and the expectation value of the energy ϵ_{0l} numerically, we must chose a discrete collection of points (sites) along the radial direction. Hence, we calculated the ratio of sums

$$\epsilon_{0l} = \frac{\sum_{i=0}^{i_{max}-1} \Delta y\, \frac{y_i + y_{i+1}}{2} \left[\frac{\Delta R_{0l}(y)}{\Delta y}\right]_i^2 + \sum_{i=1}^{i_{max}} \Delta y\, y_i\, U_{l,i}^{eff} R_{0l,i}^2}{\sum_{i=1}^{i_{max}} \Delta y\, y_i\, R_{0l,i}^2},$$

where ΔR_{0l} are forward differences, and the values of Δy and i_{max} were chosen to ensure a big enough range of integration $Y = \Delta y\, i_{max}$ and a small enough integration interval Δy.

We then varied the wave function randomly, accepting any changes that decreased the energy. The function was varied by sweeping the sites, excluding the point at the origin but including the point corresponding to Y, where it was left free to fluctuate. At each site, the wave function was changed by adding to it a random number in the interval $[-\varepsilon, \varepsilon)$. After a certain number of sweeps (blocks), the position of the maximum was determined and the function was renormalized to keep constant its maximum value.

During the sweeping procedure we monitored the *acceptance rate* of the trial changes in the wave function, which depends strongly on the value chosen for the range ε. In order to keep the code efficient, it is necessary to ensure that the wave function is being changed as fast as possible. The optimum value for ε is the one which maximizes the product of this range by the acceptance rate. This product is a good estimator for the overall speed with which the wave function is being modified. We included in the code a feedback mechanism which searched for this optimum value of ε by maximizing the product.

The runs were started with a large value for ε, which was then continuously adjusted by the code as the run proceeded. We found that the feedback mechanism worked very well to decrease ε to appropriate values but that sometimes it could overshoot and get hung at extremely small values of the range. This was particularly true in the long runs needed for the precise determination of the binding energies. This problem was overcome by a procedure which we call *quenching*. We stopped the runs two or three times, storing

the wave function produced so far, and restarted them with a large value for the range ϵ. This procedure greatly increased the convergence speed of the code. Figs. 5 and 6 display the relaxation of the binding energy and of the average radius of the bound state, at the final quenching cycle, in a particular case.

Another relevant numerical issue is a phenomenon related to the finite numerical precision of the computer. During the sweeping procedure it was often found that many changes in the wave function did not produce any changes at all in the energy. Clearly, in these cases the change in the energy was below the numerical precision available. When this happened we accepted the change anyway, monitoring separately the acceptance rates due to relaxation of the energy and to this phenomenon. The acceptance of these changes interacted with the relaxation changes, increasing the efficiency of the code. Another source of numerical errors was related to the sweeping procedure. In order to save computation time, during the blocks of sweeps, the energy was not re-calculated every time a site was upgraded, but had instead its variations added to it along the way. This introduced numerical errors in the system and, in order to keep the errors small, after each block of sweeps the energy was calculated anew.

The finite-precision phenomena described above caused a small random drift in the results, which were used to estimate the stochastic errors. The stability of the results was tested against variations of Y and Δy. Due to the exponential decay of the wave function for large y, it was found that, given a large enough Y, the results were essentially independent of it. They were somewhat more sensitive to the finiteness of Δy, approaching a limit linearly with Δy, as $\Delta y \to 0$. Also, the code became progressively less efficient as one decreased Δy. The reason for this is easily understood. For small Δy any change in the wave function at a single site tends to produce large spikes in its derivative and, then, the derivative term of the energy causes all but very small changes to be rejected. For small Δy the local upgrading is inefficient to change the long-wavelength components of the configurations.

Being prevented by the computational limitations from decreasing Δy indefinitely, we estimated the $\Delta y = 0$ limits of the results by linear regression to zero from three finite-Δy runs, for each set of values of the parameters β_{in} and l. These are the data presented in Figs. 7–11. They were calculated assuming m to be the usual electron mass. The energy eigenvalues for $l = -5$ and $l = -7$ are very close to those corresponding to $l = -3$ and $l = -1$, respectively, and for this reason they have not been included in the figures. The error bars are too small to be visible in the graphs. The stars mark the points calculated directly, while the lines were obtained by splines interpolations. The corresponding dissociation temperatures $T_{d,nl}$ are plotted in Fig. 9. Table 1 contains approximate fits for the data.

An examination of U_l^{eff} in Eq. (20) shows that for large y the potential changes very little between the cases $l = -3$ and $l = -5$, and between the cases $l = -1$ and $l = -7$. The dominant term $l(l+8)/y^2$ does not change at all; the only term that does change contains K_1, which is exponentially damped for large y. It is not so clear how much the potential changes near the well, which is the most important region as far as the bound states are

concerned. In fact, one finds but very small differences between the energies for $l = -3$ and $l = -5$, and between those for $l = -1$ and $l = -7$. The ground state of the system is the $l = -3$, $n = 0$ state, but the $l = -5$, $n = 0$ state is very close to it, forming a quasi-degenerate doublet.

Assuming that transitions between these states do occur, the transition energy would correspond to very low resonant frequencies, in the radio spectrum. This resonant frequency f_R appears in Fig. 10, as a function of β_{in}, and in Fig. 11, as a function of the dissociation temperature. Presumably, the states with larger n also form similar doublets and there should be further transition frequencies, similar to this one, corresponding to them.

5 Conclusions

There are ranges of the parameters l and β_{in} where the results of Sec. 4 are numerically consistent with the observed phase-transition temperatures of high-T_c superconductors. We do not think that this fact is merely accidental, although we are not claiming that QED_3 appropriately describes all features of high-T_c superconductivity. Also note that if the initial state of the system contains only low energy electrons, energy conservation forbids the production of electron-positron pairs. No electron-positron bound states can be formed and, as a consequence, only the electron-electron bound state can characterize the many-body ground state.

Certainly, the calculations presented here are still incomplete. For instance, one should recalculate the potential for the finite-temperature field theory, which presumably will introduce corrections in the energies and temperatures. It also remains to be shown that the theory exhibits a phase transition and that the many-body ground state is a condensate of electron-electron pairs. However, if this turns out to be the case, we find reasonable to think that the dissociation temperatures found in this paper should be, at least, rough approximations for the true phase-transition temperatures.

We believe that the accidental quasi-degeneracy uncovered in this work may be important to test the relevance of the model for the description of high-T_c superconductors. The corresponding transition frequency is directly related to the binding energy of the ground state, and therefore to the predicted dissociation temperature. The relation thus implied, between this frequency and the phase-transition temperature, may provide a means of testing the applicability of the model for the description of high-T_c superconductors. If the model considered here is more than superficially related to high-T_c superconducting materials, it should be possible to detect such a transition. It certainly would be very interesting to further pursue this matter.

Acknowledgements

One of us (AJS) thanks Prof. R. Jackiw for many valuable criticisms, and the Center for Theoretical Physics of MIT for the kind hospitality. The computer work presented in this paper was realized mostly on the Unix computer systems of the "Departmento de Física Matemática", which were acquired with grants from Fapesp. The computer systems of the "Instituto de Física" were also used.

References

[1] S. Deser, R. Jackiw and S. Templeton, Ann. Phys. (NY) **140** (1982) 372.

[2] H. O. Girotti, M. Gomes and A. J. da Silva, Phys Lett. **B274** (1992) 357.

[3] Ya. I. Kogan, JETP Lett. **49**, 225 (1989).

[4] For a similar derivation of the effective electron-electron potential arising from QED_4 see, for instance, J. J. Sakurai, "Advanced Quantum Mechanics" (Addison-Wesley, Mass., 1967); A. I. Akhiezer and V. B. Berestetskii, "Quantum Electrodynamics" (John Wiley, N. Y., 1965).

[5] F. Bloch and A. Nordsieck, Phys. Rev. **52** (1937) 54.

[6] N. N. Bogoliubov and D. V. Shirkov, "Introduction to the Theory of Quantized Fields" (John Wiley, N. Y. , 1980).

[7] A. V. Svidzinskiy, JETP **31** (1956) 324.

[8] R. Jackiw and L. Soloviev, Phys. Rev. **173** (1968) 1485.

[9] A. N. Redlich, Phys. Rev. Lett. **52** (1983) 18; Phys. Rev. **D29** (1984) 2366.

[10] H. O. Girotti, M. Gomes and A. J. da Silva, preprint IFUSP/P-977 (1992); H. O. Girotti, M. Gomes, J. L. deLyra, R. S. Mendes, J. R. S. Nascimento and A. J. da Silva, preprint IFUSP/P-986 (1992).

[11] I. Kogan, Phys. Lett. **B262**, 83 (1991); I. Kogan and G. W. Semenoff, Nucl. Phys. **B368**, 718 (1992).

FIGURES

1. Wavy lines represent free photons, while dashed lines refer to massive vector particles.

2. The vertex insertion Λ^{μ}.

3. Diagrams contributing to the potential $\Delta V^{\mathrm{QED}_3}$.

4. The bound-state wave function R_{0l} (dashed line) and the dimensionless potential U_l^{eff} (continuous line) for $l = -3$, $\beta_{in} = 2000$, $\Delta y = 0.25$ and $Y = 200$. The vertical scale refers only to the potential. The normalization of the wave function is arbitrary.

5. Relaxation of the dimensionless energy parameter ϵ_{0l} for $l = -3$, $\beta_{in} = 2000$, $\Delta y = 0.25$ and $Y = 200$, on the last quenching run, as a function of the blocks of sweeps. The vertical scale is relative to the minimum value $\epsilon_{0-3} = -0.03266121075526209$, which corresponds to the zero of the scale.

6. Relaxation of the dimensionless average radius $\bar{y}_{0l}$ for $l = -3$, $\beta_{in} = 2000$, $\Delta y = 0.25$ and $Y = 200$, on the last quenching run, as a function of the blocks of sweeps. The vertical scale is relative to the mean value $\bar{y}_{0-3} = 18.02868690614052$, which corresponds to the zero of the scale.

7. Binding energy E_{0l}, in eV, versus the dimensionless parameter β_{in}, for $l = -1$ and $l = -3$.

8. Average radius $\bar{r}_{0l}$, in Å, versus the dimensionless parameter β_{in}, for $l = -1$ and $l = -3$.

9. Dissociation temperature $T_{d,0l}$, in K, versus the dimensionless parameter β_{in}, for $l = -1$ and $l = -3$.

10. Resonant frequency f_R, in MHz, versus the dimensionless parameter β_{in}, for the $(l = -3)$—$(l = -5)$, $n = 0$ doublet.

11. Resonant frequency f_R, in MHz, versus the dissociation temperature $T_{d,0l}$, in K, for $l = -3$.

TABLES

1. Approximate fits for the numerical data.

Graph	Fits	
$E_{0l} \times \beta_{in}$	$E_{0-1} \approx 2.25 \times 10^4 \, \beta_{in}^{-2.224} \, eV$	$E_{0-3} \approx 9.55 \times 10^4 \, \beta_{in}^{-2.229} \, eV$
$\bar{r}_{0l} \times \beta_{in}$	$\bar{r}_{0-1} \approx 4.05 \times 10^{-2} \, \beta_{in}^{1.113}$ Å	$\bar{r}_{0-3} \approx 2.86 \times 10^{-2} \, \beta_{in}^{1.117}$ Å
$T_{d,0l} \times \beta_{in}$	$T_{d,0-1} \approx 2.61 \times 10^8 \, \beta_{in}^{-2.224} \, K$	$T_{d,0-3} \approx 1.11 \times 10^9 \, \beta_{in}^{-2.229} \, K$
$f_R \times \beta_{in}$	$f_R \approx 1.29 \times 10^{13} \, \beta_{in}^{-3.465} \, MHz$	
$f_R \times T_{d,0-3}$	$f_R \approx 1.13 \times 10^{-1} \, T_{d,0-3}^{1.554}(K) \, MHz$	

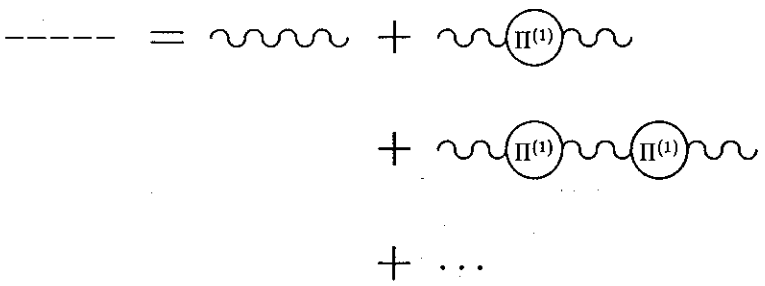

FIG. 1

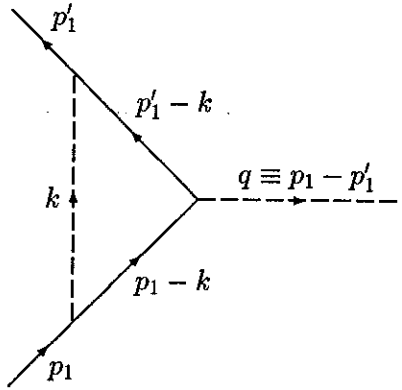

FIG. 2

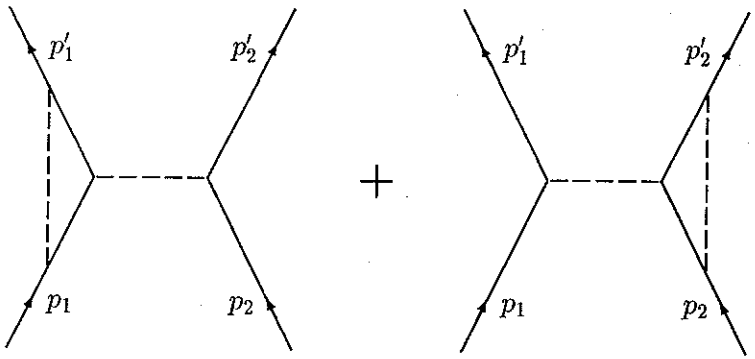
p_1'
p_2'
p_1
p_2
+
p_1'
p_2'
p_1
p_2

FIG. 3

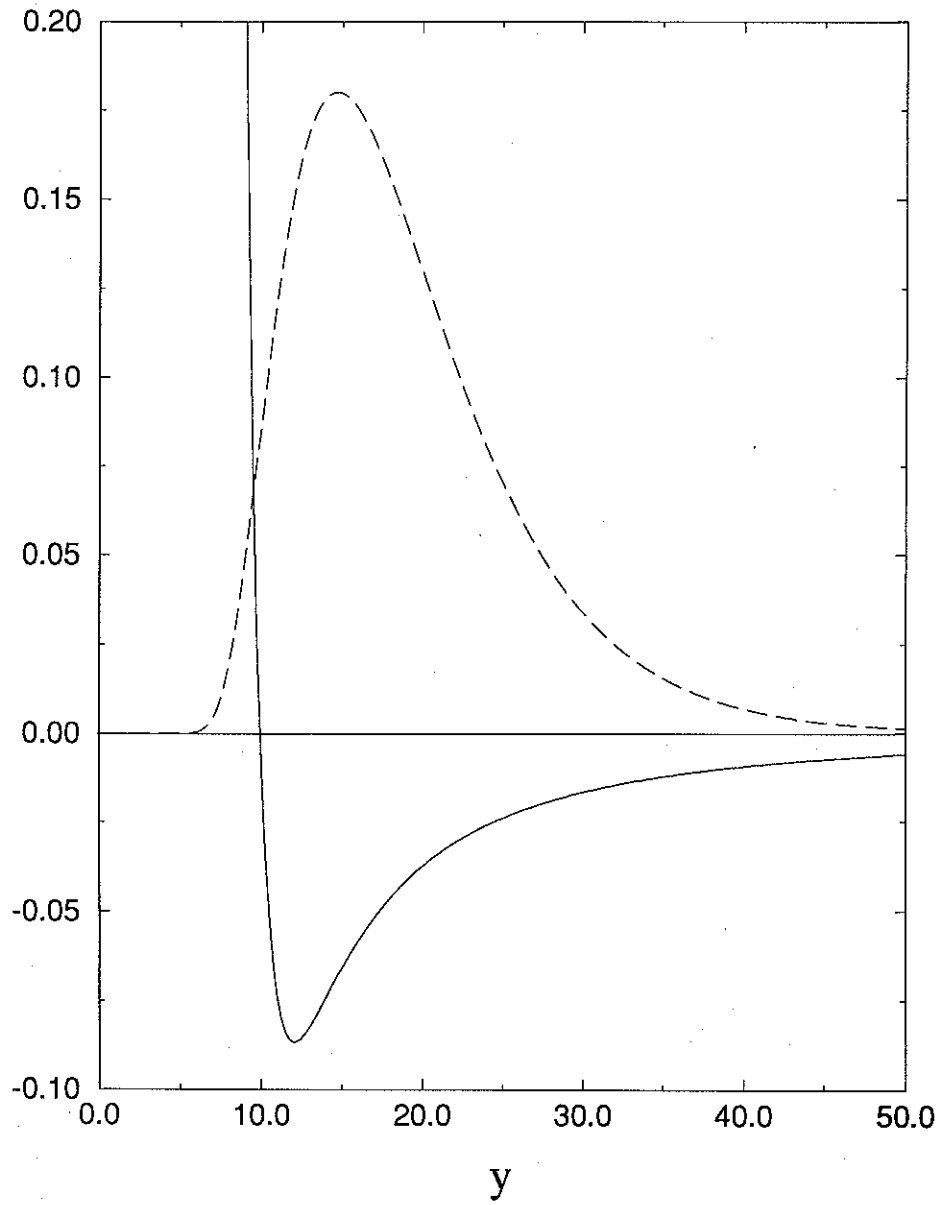
Potential and Wave Function
0.20
0.15
0.10
0.05
0.00
-0.05
-0.10
0.0
10.0
20.0
30.0
40.0
50.0
y

FIG. 4

Binding Energy

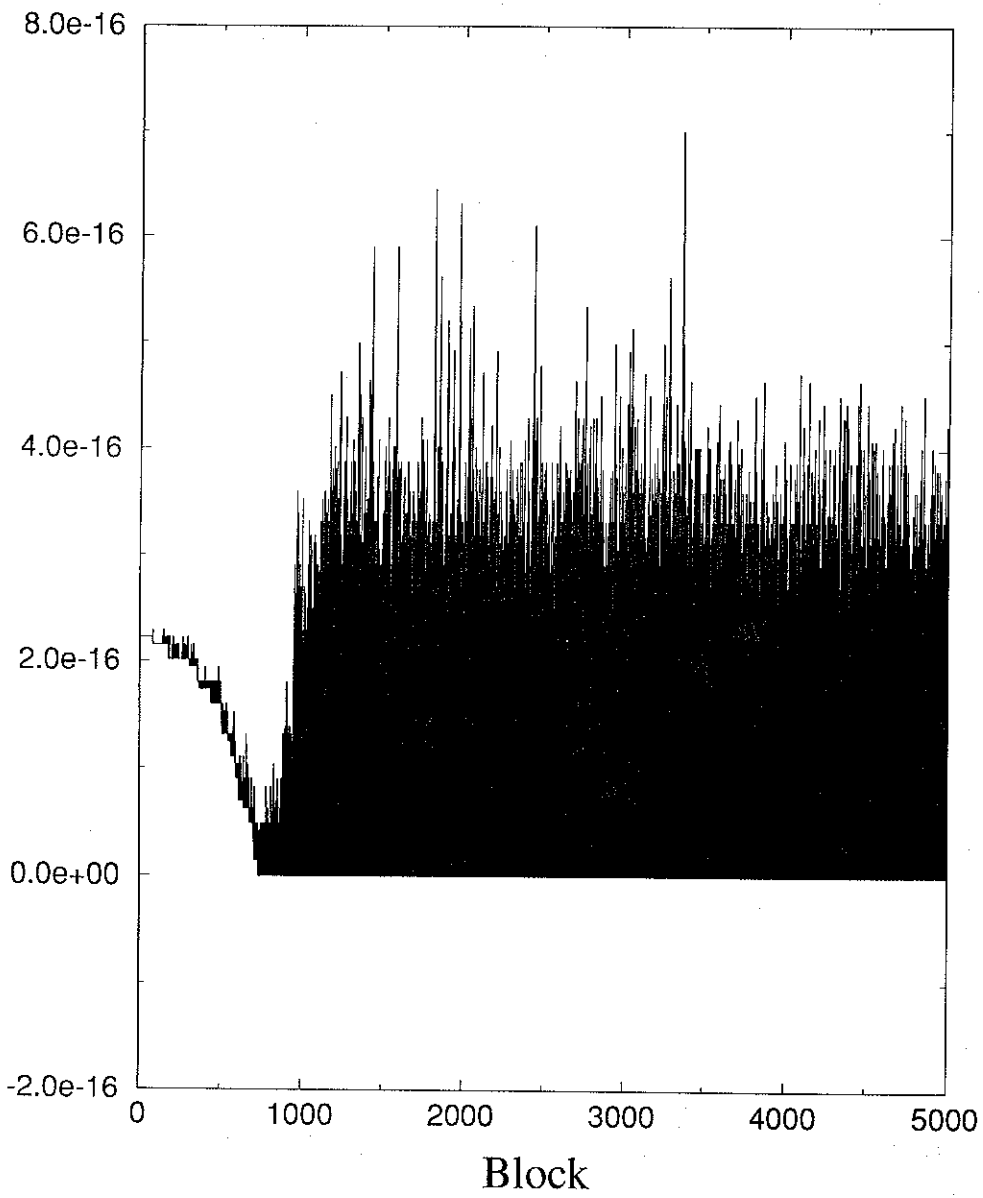

FIG. 5

Average Radius

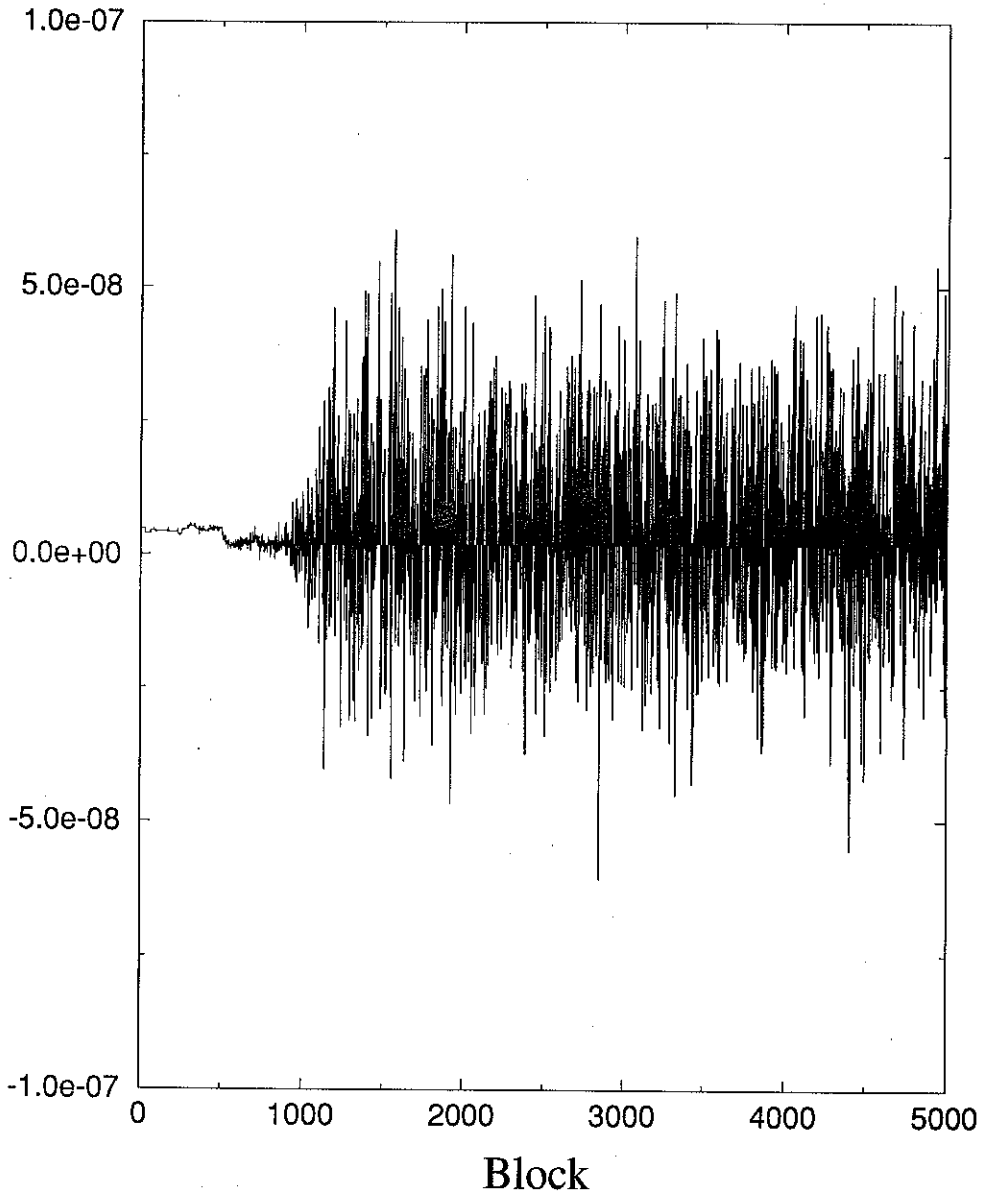

FIG. 6

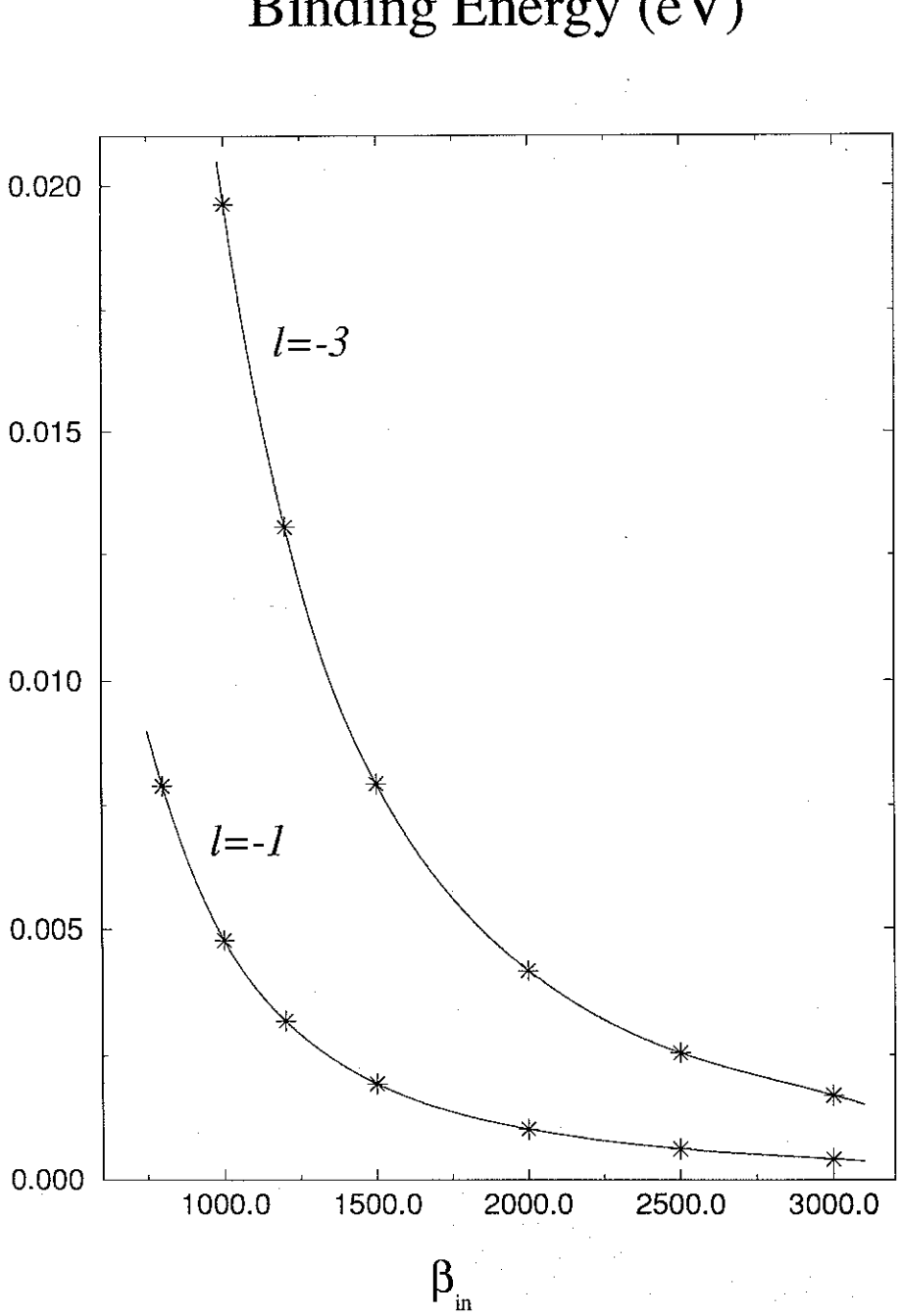
Binding Energy (eV)
0.020
0.015
0.010
0.005
0.000
l=-3
l=-1
1000.0
1500.0
2000.0
2500.0
3000.0
β in

FIG. 7

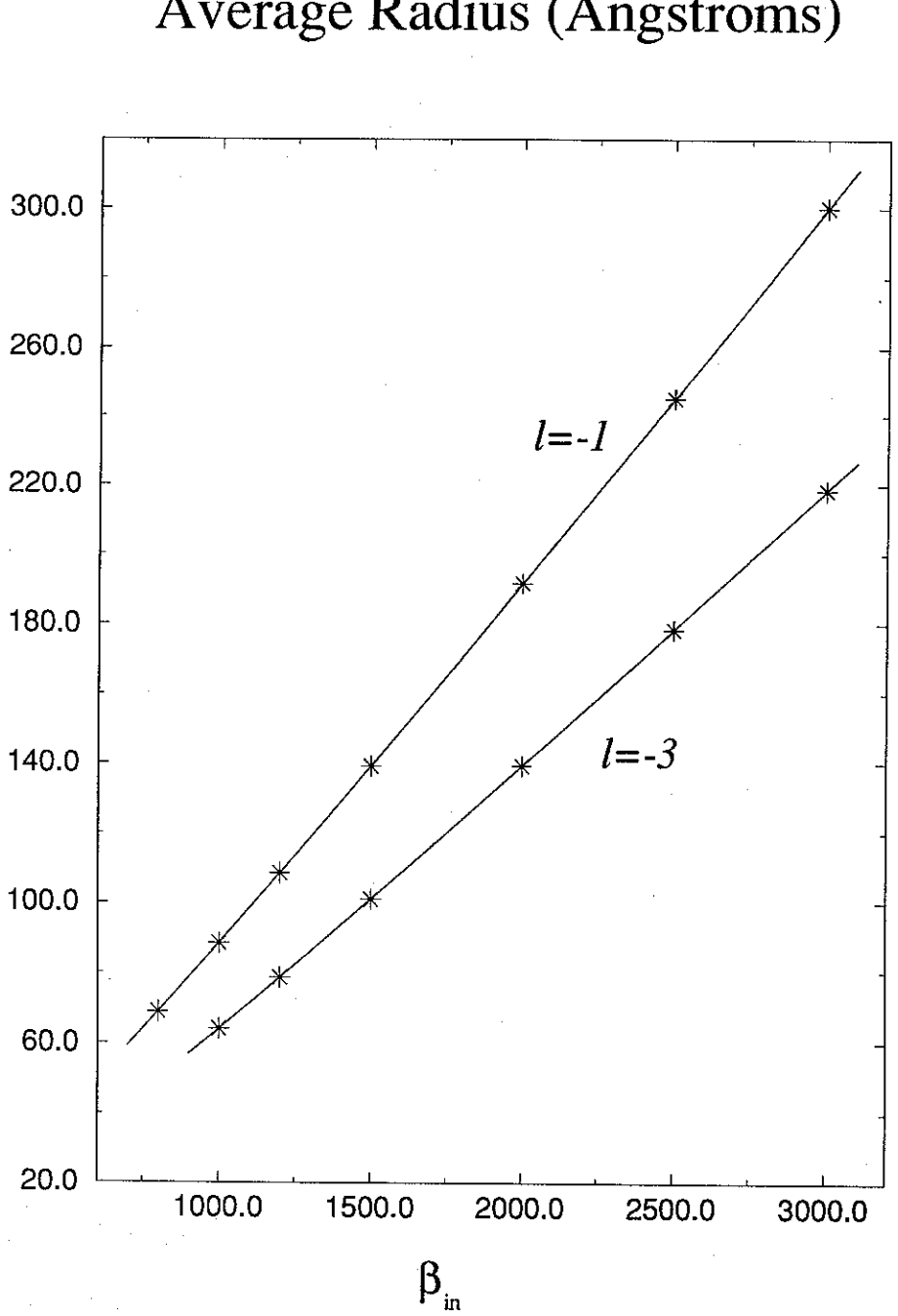
Average Radius (Angstroms)
300.0
260.0
220.0
180.0
140.0
100.0
60.0
20.0
l=-1
l=-3
1000.0
1500.0
2000.0
2500.0
3000.0
β in

FIG. 8

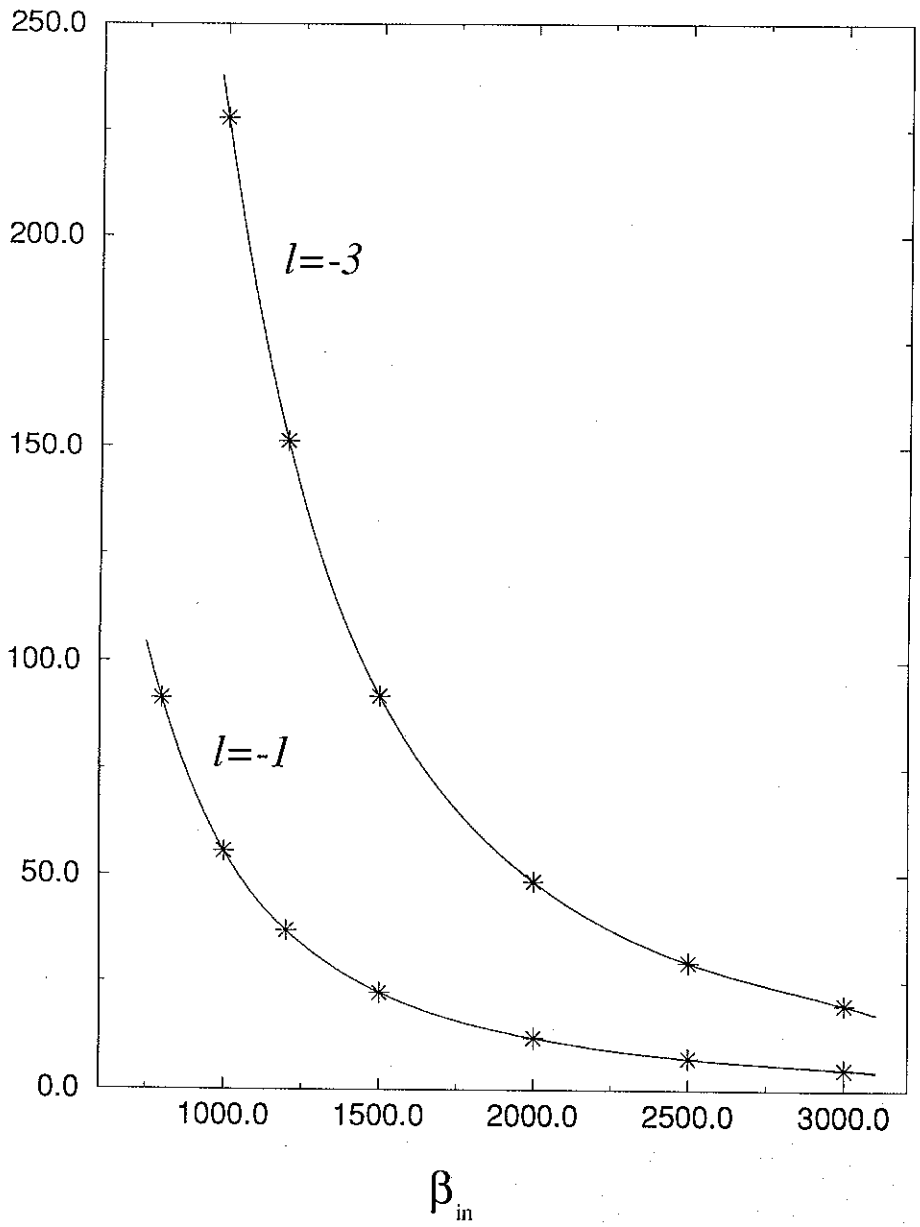
Dissociation Temperature (K)
250.0
200.0
150.0
100.0
50.0
0.0
l=-3
l=-1
1000.0
1500.0
2000.0
2500.0
3000.0
β in

FIG. 9

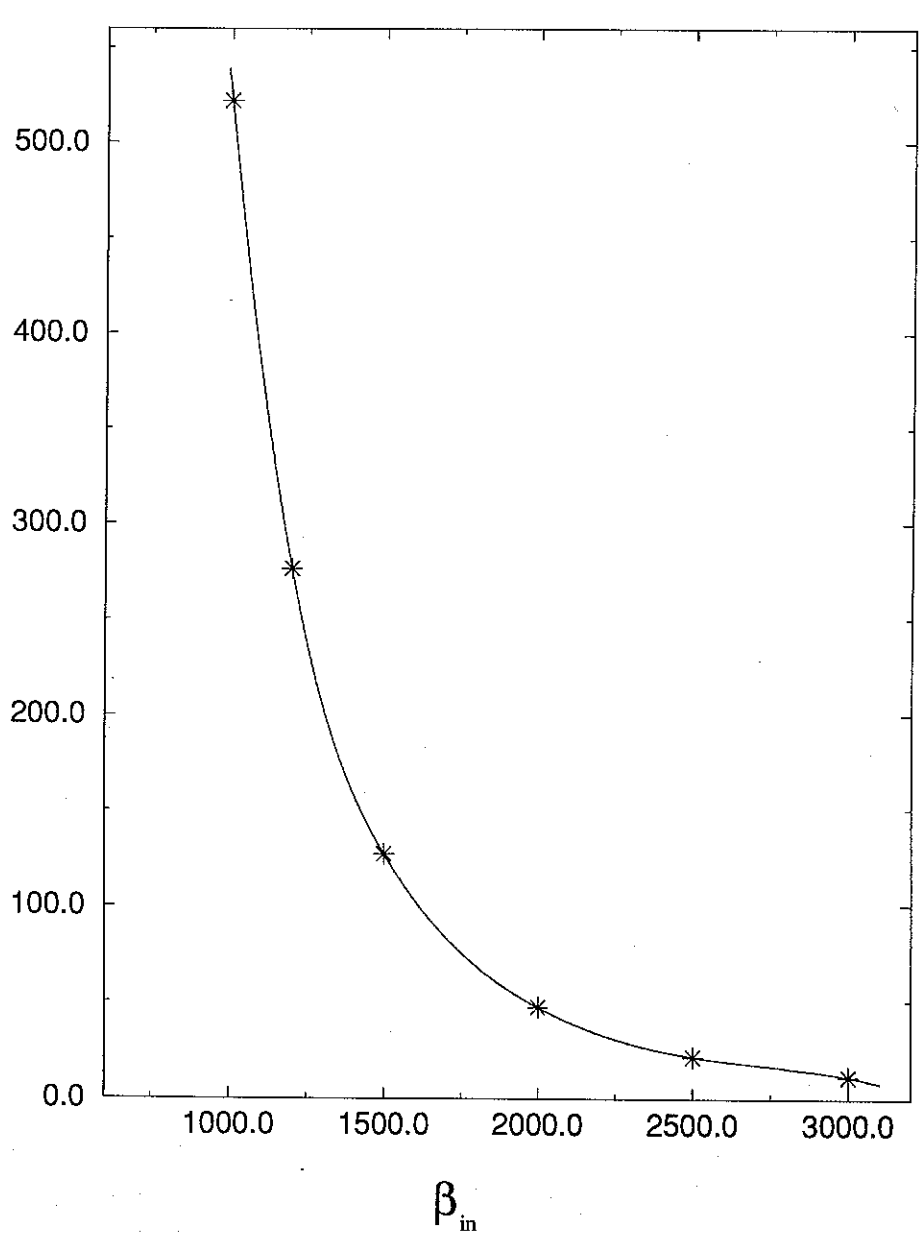
Resonant Frequency (MHz)
500.0
400.0
300.0
200.0
100.0
0.0
1000.0
1500.0
2000.0
2500.0
3000.0
β in

FIG. 10

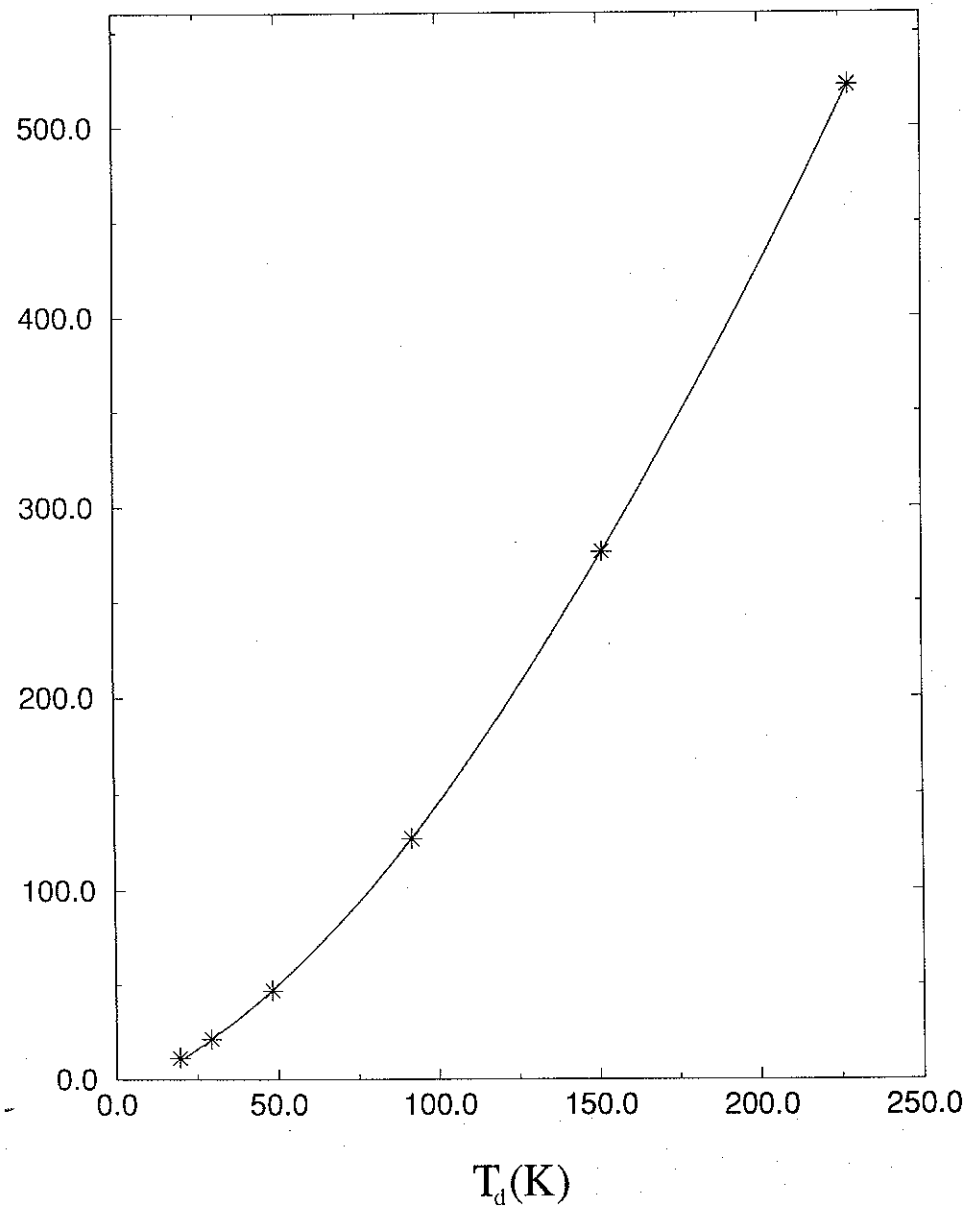
Resonant Frequency (MHz)
500.0
400.0
300.0
200.0
100.0
0.0
0.0
50.0
100.0
150.0
200.0
250.0
T_d(K)

FIG. 11